SIAM REVIEW
Vol. 60, No. 3, pp. 000–000

Pattern Formation in a Reaction-Diffusion System with Space-Dependent Feed Rate*

Theodore Kolokolnikov†
Juncheng Wei‡

Abstract. We develop novel mathematical techniques to study spot patterns in reaction-diffusion systems with space-dependent feed rate. The techniques are illustrated on the Schnakenberg model, which is a prototypical model of spot formation. Previous works have mostly addressed spot formation assuming the feed rate A is a constant, in which case the spots are uniformly distributed throughout the domain. By contrast, the spatially dependent feed rate $A(x)$ occurs naturally in applications, and very few studies exist in this case. In this work we determine analytically how this inhomogeneity affects spot creation, spot density, and spot death. We characterize the asymptotic density of spots and their heights for any spatially dependent feed rate $A(x)$. We also demonstrate a novel phenomenon which only happens when the feed rate is sufficiently inhomogeneous in space. Namely, new spots are continuously created in regions of high feed rate, travel toward regions of lower feed rate, and are destroyed there. This "creation-destruction loop" is only possible in the presence of heterogeneity. A key new technique is the Euler–Maclaurin formula to estimate the effective spike density. For a sufficiently large feed rate, we find that the effective spot density scales like $A^{2/3}(x)$, whereas the spot mass scales like $A^{1/3}(x)$. We derive asymptotic bounds for the existence of N spots. As the feed rate is increased, new spots are created through self-replication, whereas the spots are destroyed as the feed rate is decreased. The thresholds for both spike creation and spike death are computed asymptotically.

Key words. Schnakenberg model, Hopf bifurcation, mean first passage time, reaction-diffusion, matched asymptotics

AMS subject classifications. 35B36, 92C15

DOI. 10.1137/17M1116027

1. Introduction.

Reaction-diffusion PDEs are ubiquitous as models of pattern formation in a variety of biological and social systems. Some prominent examples are animal skin patterns [23, 5, 25], vortex lattices in Bose–Einstein condensates [1, 4], patterns in chemical reactions [12, 31, 19], crime hot spots in a model of residential burglaries [41, 50, 22, 8], and vegetation patches in arid environments [17, 38, 40, 9]. A common feature of many of these systems is the presence of localized patterns such

*Received by the editors February 13, 2017; accepted for publication (in revised form) September 26, 2017; published electronically August 8, 2018.
http://www.siam.org/journals/sirev/60-3/M111602.html
Funding: The work of the first author was supported by NSERC Discovery Grant RGPIN-33798 and Accelerator Supplement Grant RGPAS/461907. The work of the second author was supported by NSERC Discovery Grant RGPIN-XXXX and Accelerator Supplement Grant RGPAS/XXXX.

†Department of Mathematics and Statistics, Dalhousie University, Halifax, NS, B3H 3J5, Canada (tkolokol@mathstat.dal.ca).
‡Department of Mathematics, University of British Columbia, Vancouver, BC, V6T 1Z2, Canada (jcwei@math.ubc.ca).

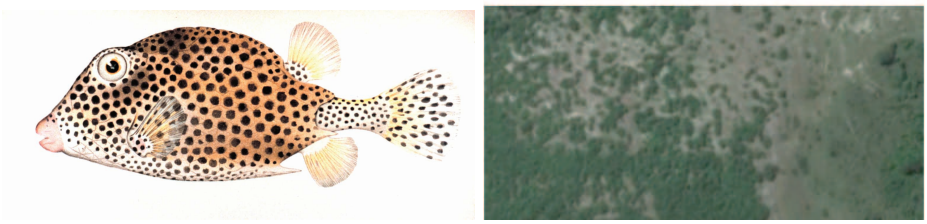

Fig. 1 *Left: Space-dependent density of spots on a fish. Right: height-dependent distribution of vegetation patterns on a mountainside near L'Aquila, Italy. Image taken from Google Earth.*

as spots, stripes, etc. There is a very large literature about the formation and stability of these patterns, especially within homogeneous environments. We refer the reader to the books [34, 16, 10, 28, 44] and references therein.

While initial pattern formation and various instabilities are by now well studied, much less is known about the distribution of resulting patterns, especially—as is often the case in nature—if there are spatial inhomogeneities. For example, vortex crystals in Bose–Einstein condensates form in the presence of a rotating confining trap, which is modeled by the Gross–Pitaevskii equation with a space-dependent potential [11]. The condensates are not uniformly distributed but have a higher density near the center of the trap [37, 2, 18]. Animal skin patterns are also highly dependent on the location within the animal, since the thickness, curvature, and growth of the skin are nonuniform and have a large effect on the resulting patterns [27, 35, 32, 6, 24, 45]. Similarly, the distribution of vegetation patches is highly dependent on the amount of precipitation and slope gradients, which vary in space and time [9, 42, 39]. See Figure 1 for some examples.

In this paper we study the spot distribution and stability of a one-dimensional reaction-diffusion model with a space-dependent feed rate. For concreteness, we concentrate on the well-studied Schnakenberg model [36, 15, 43], but we anticipate that these techniques can be extended to other settings. We consider the following limiting scaling of the Schnakenberg model:

$$\text{(1.1)} \qquad \begin{cases} \varepsilon^2 u_t = \varepsilon^2 u_{xx} - u + u^2 v, & x \in (-L, L)\,, \\ 0 = v_{xx} + a_0 A(x) - \dfrac{u^2 v}{\varepsilon}, & x \in (-L, L)\,, \\ u_x = 0 = v_x \text{ at } x = \pm L. \end{cases}$$

These equations model the following process: a fast-diffusing substrate v is consumed via the reaction $2u + v \to 3u$ by a slowly diffusing activator u, which decays with time. The substrate is being pumped into the system at some space-dependent feed rate $a_0 A(x)$. The constant a_0 represents the overall feed strength, and we will use it as the control parameter. The reaction kinetics for u and v occur at different scales: u reacts much slower than v, so that v is effectively slave to u. For simplicity of presentation, we assume that only the feed rate $A(x)$ is space dependent. However, the techniques of this paper can be generalized to incorporate space dependence into other parameters, such as the consumption or decay rate of the activator. We also disregard any potential time dependence of the parameters. This is left for future work.

The full Schnakenberg model also has an additional term in the equation for v : $\tau v_t = v_{xx} + a_0 A(x) - \frac{u^2 v}{\varepsilon}$, where τ represents the "reaction time" of v relative

to u. The results presented in this paper are unchanged as long as $\tau \ll O(\varepsilon^{-1})$; this corresponds to having a sufficiently fast response of v to u. On the other hand, if τ is sufficiently increased, oscillatory instabilities are triggered that have destabilizing and very complex effects on resulting patterns [48]. The analysis of these instabilities is beyond the scope of this paper.

This model is a limiting case of the Klausmeyer model of vegetation (where u represents plant density, v represents water concentration in soil, $a_0A(x)$ is the precipitation rate, and v_{xx} is replaced by $v_{xx}+cv_x-dv$) as well as the Gray–Scott model (where v_{xx} is replaced by $v_{xx}-dv$). As such, the Schnakenberg model is among the simplest prototypical reaction-diffusion models.

In the limit $\varepsilon \to 0$, the system (1.1) is well known to generate patterns consisting of spots (or spikes) [15, 43, 32], corresponding to high localized concentrations of the chemical u, as shown in Figure 2(a). In the case of the Klausmeyer model, these spots represent localized patches of vegetation. In particular, Figure 1(b) shows an example of nonuniform distribution of vegetation patches; the vegetation is more dense near the bottom of the mountain and less dense near the top. The goal of this paper is to describe the density distribution of spikes and their stability in situations like this.

We now illustrate our main results, referring to Figure 2. There, we take $A(x) = 1 + 0.5\cos(x)$ with $L = \pi$ and either decrease or increase a_0 very slowly. For a fixed a_0 and a fixed number of spikes, N, as illustrated in Figure 2(a), our theory (see Main Result 2.2 below) yields both the effective spike density and the envelope for spike heights. Note that the spike density is not uniform—it is higher at the center than at the boundaries—and the asymptotics recover the effective spike density very well. As a_0 is increased, new spikes are created through self-replication near the center (where $A(x)$ is at a maximum)—see Figure 2(b,c). On the other hand, as a_0 is decreased, spikes are destroyed near the boundary (where $A(x)$ is at a minimum) as a result of competition or coarsening instability, as shown in Figure 2(d,e). In Main Result 3.4 we show that N spikes are stable if and only if the feed strength a_0 lies within the range

$$\alpha N^{3/2} < a_0 < \beta N\varepsilon^{-1/2}, \quad \alpha = 0.504, \quad \beta = 0.38097. \tag{1.2}$$

Moreover, spike destruction occurs when a_0 is decreased below the curve $a_0 = \alpha N^{3/2}$ (dashed curve in Figure 2(e), and spike creation occurs when a_0 is increased above the line $a_0 = \beta N\varepsilon^{-1/2}$ (dashed line in Figure 2(c)).

The two boundaries $a_0 = \alpha N^{3/2}$ and $a_0 = \beta N\varepsilon^{-1/2}$ in (1.2) intersect when $a_0 = a_{0,\max} \equiv \beta^3/\alpha^2\varepsilon^{-3/2}$, and there is no stable spiky steady state that exists for $a_0 > a_{0,\max}$. However, for values of a_0 just above $a_{0,\max}$, very complex dynamics are observed, as shown in Figure 2(f): new spikes are continually being created near the center and then move toward the boundaries and are destroyed there, resulting in an infinite creation-destruction loop. In Figure 2(f), we took $\varepsilon = 0.05$ so that $a_{0,\max} = 19.469$, whereas $a_0 = 20$ is taken just above $a_{0,\max}$ (numerical simulations confirm that no such dynamics occur if $a_0 = 19$). Such a complex dynamical loop is only possible for an inhomogeneous feed rate, since the place of destruction must differ from the place of creation. We remark that this phenomenon was also previously reported in [32] and seems to be commonplace in reaction-diffusion systems with varying parameters.

The summary of the paper is as follows. The equilibrium spike density is derived in section 2. Stability is derived in section 3. We conclude with some discussions and open problems in section 4.

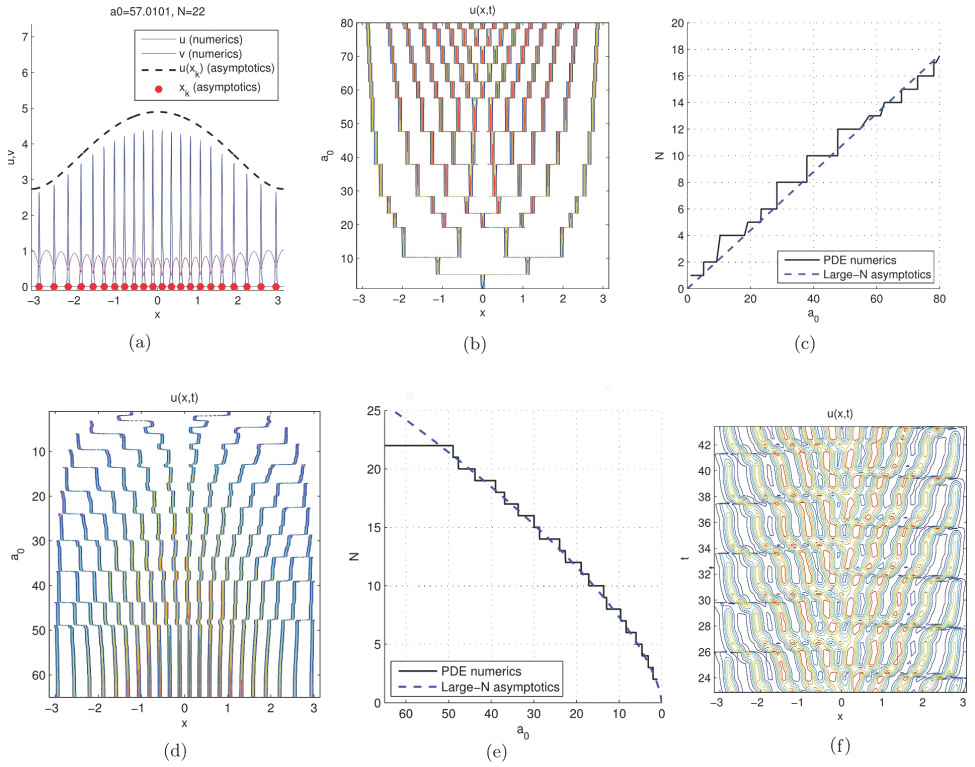

Fig. 2 (a) *Stable equilibrium configuration with* 22 *spikes. Red dots and dashed line are the theoretical prediction for the density and spike heights, as given in Main Result* 2.2. *Here,* $A(x) = 1 + 0.5\cos(x)$, $L = \pi$, $\varepsilon = 0.007$, *with* a_0 *as shown. Note that the steady state is nonuniform, unlike the case of constant* a *(see Figure* 4*).* (b) *Illustration of spike creation. Full numerical simulation of* (1.1) *where* a_0 *is gradually increased according to the formula* $a_0 = 1 + 0.08t$*; other parameters are as in* (a). *New spikes are created through self-replication near the origin, where* $a(x)$ *has its maximum.* (c) *The number of spots as a function of* a_0. *Solid stair line corresponds to the observed number of spots from the numerical simulation in* (a). *Dashed line is the theoretical prediction* $a_0 = a_{0,split}$ *given in* (3.9). (d) *Illustration of spike destruction. As in* (b) *except that* a_0 *is very gradually decreasing according to the formula* $a_0 = 120 - 0.08t$. *Note that spikes are destroyed near* $x \sim \pm\pi$. (e) *The number of spots as a function of* a_0. *Solid stair line corresponds to the observed number of spots from the numerical simulation in* (a). *Dashed line is the theoretical prediction* $a_0 = a_{0,coarse}$ *given in* (3.9). (f) *Creation-destruction loop with* $A(x) = 1 + 0.5\cos(x), a_0 = 20, \varepsilon = 0.05$. *New spikes are created near the center and are destroyed near the edges.*

2. Spike Density.

The starting point for computing spike density and stability is to derive the reduced dynamics for spike centers. By now, this is a relatively standard asymptotic computation; see, for example, [13]. For completeness, we include a self-contained derivation of spike dynamics in Appendix A. We summarize it as follows.

PROPOSITION 2.1. *Consider the Schnakenberg system* (1.1). *Assume that* $A(x)$ *is even on the interval* $[-L, L]$. *Define* $P(x)$ *and* b *by*

$$P''(x) = A(x) \quad \text{with} \quad P'(0) = 0, \qquad b \equiv 6N^3/a_0^2. \tag{2.1}$$

Assume $\varepsilon N \ll 1$. *The dynamics of* N *spikes are asymptotically described by the ODE*

system

$$\frac{dx_k}{dt}\frac{S_k}{18N} = \frac{1}{N}\sum_{\substack{j=1,\dots,N\\ j\neq k}} \frac{S_j}{2}\frac{x_k - x_j}{|x_k - x_j|} - P'(x_k) \tag{2.2a}$$

subject to $N+1$ *algebraic constraints*

$$\frac{b}{N^2}\frac{1}{S_k} = \frac{1}{N}\sum_{j=1}^{N} S_j \frac{|x_k - x_j|}{2} - P(x_k) + c, \quad k = 1,\dots,N, \tag{2.2b}$$

$$\frac{1}{N}\sum_{j=1}^{N} S_j = \int_{-L}^{L} A(x)dx. \tag{2.2c}$$

Here, x_k *is the center of the* k*th spike and* $S_k > 0$ *is proportional to its height, so that near* x_k*, the quasi-steady state is approximated by*

$$u(x) \sim \operatorname{sech}^2\left(\frac{x - x_k}{2\varepsilon}\right)\frac{S_k}{4N}, \quad v(x) \sim \frac{6N}{S_k}, \quad |x - x_k| \ll 1. \tag{2.3}$$

The next step is to construct a continuum-limit approximation for spike density. Setting $\frac{dx_k}{dt}$ to zero in (2.2a), we obtain the steady state equations

$$0 = \frac{1}{N}\sum_{j\neq k} \frac{S_j}{2}\frac{x_k - x_j}{|x_k - x_j|} - P'(x_k), \tag{2.4a}$$

$$\frac{b}{S_k}\frac{1}{N^2} = \frac{1}{N}\sum_{j} S_j \frac{|x_k - x_j|}{2} - P(x_k) - C, \quad \frac{1}{N}\sum S_j = 2P'(L). \tag{2.4b}$$

A posteriori analysis shows that N spikes are *unstable* if $b \gg 1$ (in the limit of large N), so that the relevant regime to consider is when $b = O(1)$.

To study the large-N limit, we define the *spike density* $\rho(x)$ to be a density distribution function for spikes, that is, for any $a, b \in [-L, L]$ we define $\rho(x)$ to be

$$\int_a^b \rho(x)dx \sim \frac{\#\text{ of spikes in the interval } [a,b]}{N}. \tag{2.5}$$

An alternative definition is to define

$$\rho(x) = \frac{1}{N}\sum \delta\left(x - x_j\right).$$

In the large-N limit, we consider the spike locations x_j to be a continuous function $x_j = x(j)$ from $[0, N]$ to $[-L, L]$. In terms of $x(j)$, the density may also be expressed as

$$\rho(x(j)) = \frac{1}{Nx'(j)}, \tag{2.6}$$

which also gives a way to compute the effective density given a sequence of spike positions.

Definition (2.6) is equivalent to definition (2.5). To show the equivalence, first assume (2.6). Fix $1 \le j_1 < j_2 \le N$ and let $a = x\left(j_1\right)$ and $b = x\left(j_2\right)$. Then we have

$\int_a^b \rho(x)dx = \int_{j_1}^{j_2} \rho(x(j))x'(j)dj = \int_{j_1}^{j_2} \frac{1}{Nx'(j)}x'(j)dj = \frac{1}{N}(j_2 - j_1)$, which agrees with (2.5) since $j_2 - j_1$ is the number of spikes in the interval $[a, b]$. Conversely, assume (2.5). Then $\frac{1}{N}(j_2 - j_1) = \int_a^b \rho(x)\,dx = \int_{j_1}^{j_2} \rho(x(j))x'(j)dj$. Using the mean value theorem, we have $\int_{j_1}^{j_2} \rho(x(j))x'(j)dj = (j_2 - j_1)\rho(x(j))x'(j)$, where $j \in [j_1, j_2]$. Taking the limit $j_2 \to j_1$, we then obtain $\rho(x(j))x'(j) = \frac{1}{N}$, which shows (2.6).

We also define the strength function $S(x)$ to be such that

$$S_j = S(x(j)). \tag{2.7}$$

With these definitions, we estimate the summation terms in (2.4) using integrals. For example, we have $\sum_j S_j \frac{|x_k - x_j|}{2} \approx \int S(y)\frac{|x_k - y|}{2}\rho(y)dy$, and so on. To leading order, the continuum limit of equations (2.4) then becomes

$$\int_{-L}^{L} S(y)\rho(y)\frac{1}{2}\frac{x-y}{|x-y|}dy \sim P'(x), \tag{2.8a}$$

$$\int_{-L}^{L} S(y)\rho(y)\frac{1}{2}|x-y|\,dy \sim P(x) + C. \tag{2.8b}$$

The first thing to note is that the control parameter b is *not present* in the leading-order computation in (2.8). What's worse, equation (2.8a) is a direct consequence of differentiating (2.8b); thus, at the leading order, there is only one equation, whereas there are two unknown functions: $S(x)$ and $\rho(x)$. Nonetheless, differentiating (2.8a) and using the fact that

$$\left(\frac{1}{2}\frac{x-y}{|x-y|}\right)_x = \left(\frac{1}{2}|x-y|\right)_{xx} = \delta(x-y),$$

this leading-order computation yields the following relationship between $S(x)$ and $\rho(x)$:

$$S(x)\rho(x) = P''(x) = A(x).$$

To make further progress in determining $S(x)$ and $\rho(x)$ requires a careful estimate of the difference between the discrete sums in (2.4) and their integral approximations. This estimate is supplied by the Euler–Maclaurin formula, which we recall here. Assume that $f(n)$ is a sufficiently smooth function from $[1, N]$ to $\mathbb{R}$. Then

$$\sum_{j=1}^{N} f(j) = \int_1^N f(j)dj + \frac{1}{2}(f(1) + f(N)) + \sum_{j=1}^{K} c_j\left(f^{(j)}(N) - f^{(j)}(1)\right) + R_K, \tag{2.9}$$

where the c_j are coefficients that are related to Bernoulli numbers and the remainder, R_K, depends only on higher-order derivatives of f. Here, we only need the first two coefficients:

$$c_1 = \frac{1}{12}, \quad c_2 = 0$$

(in fact all even coefficients are zero). We now apply the Euler–Maclaurin formula to estimate the sums in (2.4). We start by estimating

$$\frac{1}{N}\sum_{j\neq k}\frac{S_j}{2}\frac{x_k - x_j}{|x_k - x_j|} = \frac{1}{N}\sum_{j=1}^{k} S(x(j)) - \frac{1}{N}\sum_{j=k}^{N} S(x(j)).$$

By changing variables $x(j) = y, dj = \frac{dy}{x'(j)} = N\rho(y)dy$, we obtain

$$\begin{aligned}\frac{1}{N}\sum_{j=1}^{k} S(x(j)) &= \int_{x_1}^{x_k} S(y)\,\rho(y)dy + \frac{1}{2N}\left(S(x_1)+S(x_k)\right)\\ &\quad + \frac{1}{12N^2}\left(\frac{S'(x_k)}{\rho(x_k)} - \frac{S'(x_1)}{\rho(x_1)}\right) + O\left(\frac{1}{N^4}\right),\\ \frac{1}{N}\sum_{j=k}^{N} S(x(j)) &= \int_{x_k}^{x_N} S(y)\,\rho(y)dy + \frac{1}{2N}\left(S(x_k)+S(x_N)\right)\\ &\quad + \frac{1}{12N^2}\left(\frac{S'(x_N)}{\rho(x_N)} - \frac{S'(x_k)}{\rho(x_k)}\right) + O\left(\frac{1}{N^4}\right),\end{aligned}$$

so that

$$\begin{aligned}\frac{1}{N}\sum_{j\neq k} S_j \frac{x_k - x_j}{|x_k - x_j|} &= \int_{x_1}^{x_N} S(y)\,\rho(y)\frac{x_k - y}{|x_k - y|}dy + \frac{1}{2N}\left(S(x_1) - S(x_N)\right)\\ &\quad + \frac{1}{12N^2}\left(\frac{2S'(x_k)}{\rho(x_k)} - \frac{S'(x_1)}{\rho(x_1)} - \frac{S'(x_N)}{\rho(x_N)}\right) + O\left(\frac{1}{N^4}\right).\end{aligned}$$

Since we assumed that the feed rate $A(x)$ is even, we seek an even steady state, so that $S(x)$ is also even and $x_1 = -x_N$. Then $S(x_1) = S(x_N)$, $\frac{S'(x_1)}{\rho(x_1)} = -\frac{S'(x_N)}{\rho(x_N)}$, and

$$\begin{aligned}\int_{x_1}^{x_N} S(y)\,\rho(y)\frac{x_k - y}{|x_k - y|}dy &= \int_{-L}^{L} S(y)\,\rho(y)\frac{x_k - y}{|x_k - y|}dy + \int_{-L}^{x_1} S(y)\,\rho(y)dy - \int_{x_N}^{L} S(y)\,\rho(y)dy\\ &= \int_{-L}^{L} S(y)\,\rho(y)\frac{x_k - y}{|x_k - y|}dy,\end{aligned}$$

so that we finally obtain

$$\frac{1}{N}\sum_{j\neq k} S_j \frac{1}{2}\frac{x_k - x_j}{|x_k - x_j|} = \int_{-L}^{L} S(y)\,\rho(y)\frac{1}{2}\frac{x_k - y}{|x_k - y|}dy + \frac{1}{N^2}\left(\frac{1}{12}\frac{S'(x_k)}{\rho(x_k)}\right) + O(N^{-4}).$$

A similar computation yields

$$\frac{1}{N}\sum_{j\neq k} S_j \frac{|x_k - x_j|}{2} = \int_{-L}^{L} S(y)\,\rho(y)\frac{|x_k - y|}{2}dy + \frac{1}{N^2}\left(-\frac{1}{12}\frac{S(x_k)}{\rho(x_k)} + C_0\right) + O(N^{-4}),$$

where C_0 is an irrelevant constant that depends on $S(\pm L), S'(\pm L)$, $\rho(\pm L)$, and $\rho'(\pm L)$.

We now expand

$$S(x) = S_0(x) + \frac{1}{N^2}S_1(x) + \cdots$$

to obtain

$$\int S_0(y)\rho(y)\frac{1}{2}\frac{x - y}{|x - y|}dy = P'(x), \quad \int S_0(y)\rho(y)\frac{1}{2}|x - y|\,dy = P(x) + C,$$

$$\int S_1(y)\rho(y)\frac{1}{2}\frac{x - y}{|x - y|}dy = -\frac{1}{12}\frac{S_0'(x)}{\rho(x)}, \tag{2.10}$$

$$\int S_1(y)\rho(y)\frac{1}{2}|x - y|\,dy = \frac{1}{12}\frac{S_0(x)}{\rho(x)} + \frac{b}{S_0(x)} + C_0. \tag{2.11}$$

Upon differentiating (2.11) and substituting into (2.10), we finally obtain the following ODE, which relates $S_0(x)$ and $\rho(x)$:

$$-\frac{1}{12}\frac{S_0'(x)}{\rho(x)} = \frac{d}{dx}\left(\frac{1}{12}\frac{S_0(x)}{\rho(x)} + \frac{b}{S_0(x)}\right). \tag{2.12}$$

Furthermore, we have

$$S_0(x)\rho(x) = A(x), \quad \int_{-L}^{L}\rho(x)dx = 1. \tag{2.13}$$

Together, the relationships (2.12) and (2.13) fully determine $S_0(x)$ and $\rho(x)$ in terms of $A(x)$.

Solving for $\rho'(x)$ from (2.12) yields a Bernoulli ODE,

$$\rho' = \frac{2S_0'}{S_0}\rho - 12b\frac{S_0'}{S_0^3}\rho^2, \tag{2.14}$$

whose solution is readily obtained as

$$\frac{S_0^2}{\rho} - 12b\log(S_0) = C. \tag{2.15}$$

Substituting $S_0 \sim S \sim A/\rho$, we find that the steady state satisfies, at leading order,

$$\frac{A^2}{\rho^3} + 12b\log(\rho/A) \sim C \ \text{ subject to } \int_{-L}^{L}\rho(x)dx = 1; \quad S\rho \sim A \text{ as } N\to\infty. \tag{2.16}$$

We summarize as follows.

Main Result 2.2. *Let x_j and S_j be the equilibrium locations of the reduced system* (2.2) *with $\partial x_j/\partial t = 0$. The spike density $\rho(x)$ as defined by* (2.5) *is asymptotically approximated by* (2.16). *The spike strengths are given by $S_j = S(x_j)$.*

An important special case of the formula (2.16) is when $b \to 0$ or, equivalently, $a_0 \gg O(N^{3/2})$. Then $\frac{A^2}{\rho^3} = C$, and, together with $\rho S = A$, we find $\rho = C_0 A^{2/3}$, $S = C_0^{-1}A^{1/3}$, where the normalization constant C_0 is determined through $\int\rho = 1$:

$$S(x) \sim \left(\int_{-L}^{L} A^{2/3}(y)dy\right)A^{1/3}(x), \qquad \rho(x) \sim \frac{A^{2/3}(x)}{\int_{-L}^{L}A^{2/3}(y)dy}. \tag{2.17}$$

Figure 2(a) shows the direct comparison between Main Result 2.2 and the full numerical simulations of (1.1); see also Figure 5(c). In fact, the agreement is very good even with a relatively small N (for example, $N = 4$; not shown). There are two sources of error when comparing the asymptotics to full numerics. The first source of error is when approximating the PDE dynamics using the reduced system (2.2), which removes the ε from the PDE. This error scales like $O(\varepsilon)$. The second source of error is made when approximating the reduced system (2.2) by its continuum limit (2.17). This error comes from the truncation of the Euler–Maclaurin series and scales like $O(1/N^2)$. In other words, the effects of nonzero ε are captured going from the PDE (1.1) to the reduced system of Proposition 2.1, while the effects due to finite N are captured in going from the reduced system of Proposition 2.1 to Main Result 2.2.

The equilibrium state with N spikes as given by Main Result 2.2 only exists for restricted parameter values. This is illustrated in Figure 2. As a_0 is increased, the steady state eventually breaks down because of spike replication. This is related to the effect of ε. As a_0 is decreased, the steady state eventually breaks down because of overcrowding effects leading to spike destruction. This is related to the effect of N. The study of this breakdown is the topic of the next section.

3. Self-Replication and Coarsening. We begin with an examination of self-replication. Numerical simulations (cf. Figure 2) show that self-replication is triggered if a_0 is sufficiently increased. This is a well-known phenomenon that was first identified in one dimension in [33] and was further studied in [26, 29, 30, 20, 21]. As explained in Appendix A, it is related to the disappearance of the the steady state for the so-called core problem as a result of a fold point bifurcation. In Appendix A we show that self-replication of the jth spot is triggered when S_j is increased past $2.70\varepsilon^{-1/2}\frac{N}{a_0}$ (see (A.20)). Moreover, suppose that $a_0 \gg O(N^{3/2})$. Then from (2.17) the maximum value of S_j is given by $\max_{x\in[-L,L]} A^{1/3}(x)\big(\int_{-L}^{L} A^{2/3}(x)dx\big)$. Replacing S_j by this maximum value and replacing the inequality in (A.20) by equality yields the following threshold.

PROPOSITION 3.1 (spike birth). *Let*

$$\beta \equiv \frac{2.70}{\max\limits_{x\in[-L,L]} A^{1/3}(x)\left(\int_{-L}^{L} A^{2/3}(x)dx\right)} \tag{3.1}$$

and suppose that $N\varepsilon \ll O(1)$. Then N spikes undergo self-replication if a_0 is increased past

$$a_{0,split} \equiv \beta N\varepsilon^{-1/2}. \tag{3.2}$$

The spike that replicates is the one closest to the maximum of $A(x)$.

The condition $N\varepsilon \ll O(1)$ is equivalent to $a_0 \gg O(N^{3/2})$ when $a_0 = O(a_{0s})$. Since the spike width is of $O(\varepsilon)$, this condition also means that the spikes are well separated from each other.

Figure 2(c,d) shows that the formula (3.2) is in excellent agreement with full numerical simulations.

Next we address the coarsening thresholds resulting in spike death that occur as a_0 is decreased. Consider the case of constant A first. Then (2.16) implies that ρ is also constant, so that $2L\rho = 1$. For fixed A and b, the first equation in (2.16) defines a curve C versus ρ, as shown in Figure 3 (left). The intersection of that curve with the vertical line $2L\rho = 1$ then determines the density ρ as a function of A. Note that $C(\rho)$ has a unique minimum which occurs at

$$b = \frac{A^2}{4\rho^3}, \tag{3.3}$$

with $C = C_{\min} \equiv 4b\,(1 - \log(4bA))$. This fold point corresponds to a zero-eigenvalue crossing. The solution branch to the left of this minimum is stable, whereas the branch to its right is unstable. The stability threshold occurs precisely at the intersection of the vertical line $2L\rho = 1$ and the curve $C(\rho)$ at this minimum (refer to Figure 3). It corresponds to setting $\rho = 1/(2L)$, $C = C_{\min}$ in (2.16), which yields $b = 2A^2L^3$ or $a_0 = 3^{1/2}(N/L)^{3/2}$, with spike death occurring when a_0 is decreased below $3^{1/2}(N/L)^{3/2}$. Combining it with Proposition 3.1, we obtain the following result.

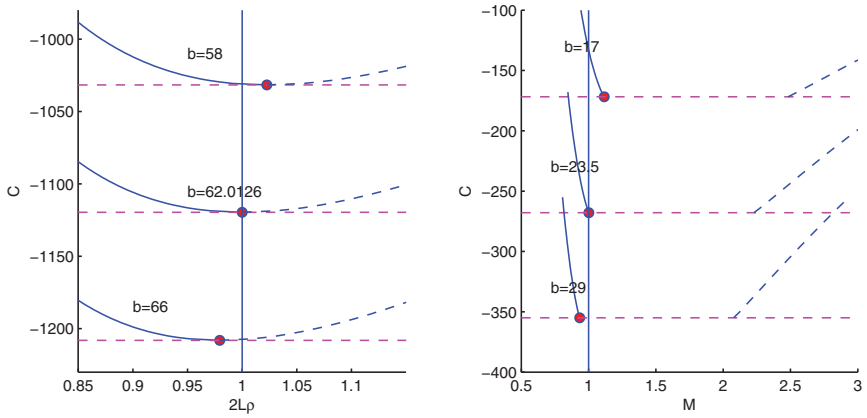

Fig. 3 *Left: the graph of C from (2.16) as a function of total mass in the case where $A(x) = A$ is constant, for three different values of b. The threshold occurs for the value of b such that the vertical line (corresponding to total mass one) intersects the curve precisely at the fold point. Right: The graph of C for nonconstant feed rate; here $A(x) = 1 + 0.5\cos(x)$. The red dot corresponds to $C_{\min}$. The threshold occurs when the red dot intersects the vertical line corresponding to a unit total mass.*

PROPOSITION 3.2. *In the case of a constant feed rate $A(x) = 1$ of the Schnakenberg model (1.1), N spikes are stable provided that*

$$3^{1/2}(N/L)^{3/2} \le a_0 \le 1.35(N/L)\varepsilon^{-1/2}. \tag{3.4}$$

Remark. In the derivation above, we have assumed that N is large. However, for a constant feed rate $A(x) = 1$, this threshold is also valid for *any* N (without assuming that N is large). It corresponds to a zero crossing of small eigenvalues [15] or, equivalently, a bifurcation point for asymmetric spike solutions [43] of the system (1.1). Let us briefly summarize the latter computation here. Consider a steady state consisting of N equal interior spikes of (1.1). Such a steady state can be obtained using even reflections of a single interior spike on a domain $[-l, l]$, where $l = L/N$. As in Appendix A, the asymptotic construction yields the outer solution of the form $v(x) \sim -a_0\frac{x^2}{2} + la_0|x| + \frac{3}{a_0 l}$, $u(x) \sim \frac{a_0 l}{3}w(x/\varepsilon)$. Now define the function $f(l) = v(x)|_{x=l} = \frac{a_0 l^2}{2} + \frac{3}{a_0 l}$. This function has a minimum at $l^3 = 3/a_0^2$. Substituting $l = L/N$ and solving for a_0 yields precisely the left-hand side of (3.4).

Figure 4 illustrates and numerically verifies the lower bound of Proposition 3.2 (see caption). Excellent agreement is observed.

We now concentrate on the inhomogeneous case. As seen in the analysis of constant A, for a given constant C and a given number A, there exist two solutions ρ of (2.16), as long as $C > 4b(1 - \log(4bA))$; the solution does not exist if the inequality is reversed. But since $A = A(x)$ varies with x, we define

$$C_{\min} \equiv 4b\left(1 - \log\left(4b \min_{x\in[-L,L]} A(x)\right)\right). \tag{3.5a}$$

Also, define $M \equiv \int_{-L}^{L}\rho$. Then (3.5a) defines a curve $C(M)$ as a function of M. For $C > C_{\min}$, there are two admissible values of M. Unlike the case of constant A (where

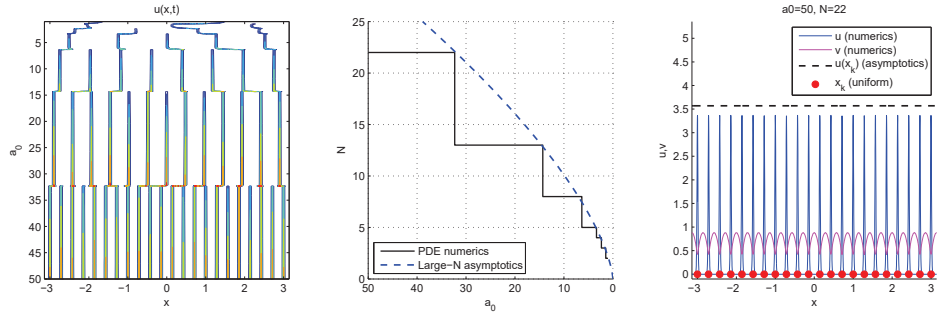

Fig. 4 *Left: spike-coarsening process with* $A(x) = 1$. *Other parameters are* $\varepsilon = 0.007$ *and* $a_0 = 50 - 0.08t$. *Middle: The number of spikes as a function of* a_0. *Solid stair line corresponds to the observed number of spots from the numerical simulation. Dashed curve is the theoretical prediction given by Main Result* 2.2. *Right: steady state consisting of* 22 *spikes.*

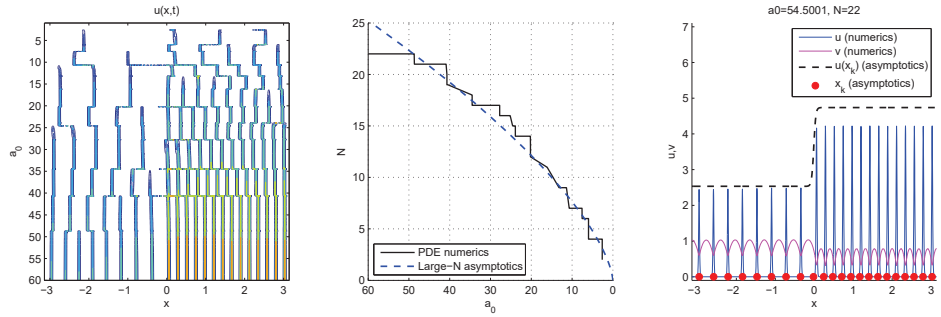

Fig. 5 *Same as Figure* 4 *except that* $A(x) = \begin{cases} 0.5, & x \in (-\pi, 0) \\ 1.5, & x \in (0, \pi). \end{cases}$

$M = 2L\rho$), not all positive values of M are admissible; a gap opens up—see Figure 3 (right). The solution to (2.16), when it exists, is the point along the curve $C(M)$ for which $M = 1$. As illustrated in Figure 3, there are two branches of the curve $C(M)$. The left branch is stable, whereas the right branch is unstable. The disappearance of the steady state occurs when $C = C_{\min}$. In other words, it is the solution to

$$\frac{A^2(x)}{\rho^3(x)} + 12b \log\left(\rho(x)/A(x)\right) = C_{\min}, \tag{3.5b}$$

where $\rho(x)$ is the smaller of the two admissible solutions, subject to the constraint

$$\int_{-L}^{L} \rho(x)dx = 1. \tag{3.5c}$$

We summarize this stability result as follows.

PROPOSITION 3.3 (spike death). *Let* b *be the solution to* (3.5) *and let* $\alpha = (6/b)^{1/2}$. *The* N*-spike equilibrium becomes unstable, resulting in spike death as* a_0 *is decreased below* $N^{3/2}\alpha$.

Interestingly, the competition threshold for any N depends only on a single universal number α, which must be computed from $A(x)$.

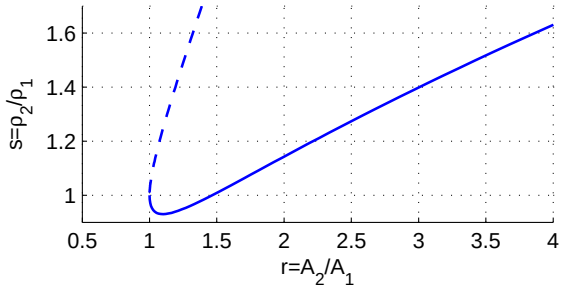

Fig. 6 *The plot of* (3.8).

To illustrate Proposition 3.3, in Figure 2(d,e) we took $A(x) = 1 + 0.5\cos(x)$ with $L = \pi$. Numerical solution to (3.5) returns $\alpha = 0.504$ (compare this with $A(x) = 1, L = \pi,\ \alpha = 0.311$). Starting initially with $N = 22$ spikes and $a_0 = 65$ and very gradually decreasing a_0, as indicated in the figure, as a_0 is decreased below $\alpha N^{3/2}$, the spikes start to disappear one by one near the boundaries where $A(x)$ is at a minimum. This is in contrast to the case of constant $A(x) = 1$, for which about half of the spikes are destroyed every time the threshold is breached (see Figure 4). Figure 2(e) shows the curve $a_0 = \alpha N^{3/2}$ in excellent agreement with full numerics.

An important special case is when $A(x)$ is piecewise constant [7, 6]. Suppose that

$$A(x) = \begin{cases} A_1, & x \in I_1, \\ A_2, & x \in I_2, \end{cases} \quad \text{with } A_1 < A_2,$$

where the the domain $[-L, L]$ is a disjoint union of I_1, I_2 whose respective size is l_1, l_2 (so that $2L = l_1 + l_2$). Straightforward algebra yields the following solution to the system (3.5):

$$\frac{r^3}{s^3} = \exp\left(\frac{r^2}{s^3} - 1\right) \qquad \text{where } r = \frac{A_2}{A_1}, \quad s = \frac{\rho_2}{\rho_1}, \tag{3.6}$$

$$b = \frac{A_1^2}{4\rho_1^3}, \qquad \rho_1 l_1 + \rho_2 l_2 = 1. \tag{3.7}$$

The relationship (3.6) can be written in parametric form as

$$s = \frac{\exp\left(\frac{2}{3}(\tau - 1)\right)}{\tau}, \qquad r = \frac{\exp(\tau - 1)}{\tau} \tag{3.8}$$

and is plotted in Figure 6. Note that there are two branches that connect to $r = 1, s = 1$. The stable branch is indicated by a solid line.

For a concrete example, take $A_1 = 0.5,\ A_2 = 1.5,\ l_1 = l_2 = \pi$, so that $r = 3$ and, from the graph in Figure 6, $s = 1.4 = \rho_2/\rho_1$. In particular, near the instability threshold, there are 1.4 as many spikes in the region where $A = 0.5$ as there are in the region where $A = 1.5$. From (3.7) we further obtain $b = 26.744$, $\alpha = 0.474$. Figure 5 shows excellent agreement with full numerics in this case.

Surprisingly, as seen in Figure 6, there is a narrow regime where the density of the spikes is *higher* in the areas of smaller feed rate. This occurs when $r = A_2/A_1 \in [1, 1.5]$.

Combining Propositions 3.3 and 3.1, we now summarize our main finding as follows.

MAIN RESULT 3.4. *Suppose that* $N\varepsilon \ll 1$. *Then* N *spikes are stable when*

$$a_{0,coarse} < a_0 < a_{0,split}, \tag{3.9}$$

where

$$a_{0,coarse} \equiv \alpha N^{3/2}; \qquad a_{0,split} \equiv \beta N \varepsilon^{-1/2}. \tag{3.10}$$

The constants α, β *are given in Propositions* 3.3 *and* 3.1, *respectively. Coarsening (spike death) occurs when* a_0 *is decreased below* $a_{0,coarse}$. *Spike splitting occurs when* a_0 *is increased above* $a_{0,split}$.

Equivalently, N *spikes are stable provided that*

$$N_{\min} < N < N_{\max}, \tag{3.11a}$$

where

$$N_{\min} \equiv a_0 \frac{\varepsilon^{1/2}}{\beta}, \quad N_{\max} \equiv \left(\frac{a_0}{\alpha}\right)^{2/3}. \tag{3.11b}$$

See Figure 2 and the introduction for an illustration of this result and a comparison with full numerics.

4. Discussion. We used the Schnakenberg model with a space-dependent feed rate to illustrate how the dynamics of N interacting spots can be analyzed by considering the large-N "mean-field" limit. For any fixed and finite N, the spot dynamics are controlled by a highly nonlinear, fully coupled differential-algebraic particle system for spot positions and their weights (2.2); this system is too complex to be tractable analytically (except in the case of constant feed rate; see [14, 13]). On the other hand, in the large-N limit we were able to fully characterize the resulting steady state as well as its stability. In this limit, the particle system is delicately balanced between the continous and discrete worlds. This required a careful use of the Euler–Maclaurin summation formula to estimate asymptotically the difference between various sums appearing in the particle system and their continuum (integral) approximations. Although we assumed that N is large in our derivation, the final results work very well even for relatively small N (for example, $N = 4$), for predicting both the correct steady state and stability thresholds.

Let us contrast our results with previous studies of spikes for homogeneous parameters. In [15, 43], spot annihilation thresholds were worked out in the case of constant feed rate $A(x) = A$ (see also [14, 13] for an earlier study where similar techniques were used to derive thresholds in the related Gierer–Meinhardt model). Our results (Proposition 3.3) generalize these thresholds to the case of a nonconstant feed rate. The previous results of constant rate A are easily recovered as special cases when A is a constant, in which case the critical threshold is $A = 3^{1/2} L^{3/2} N^{-3/2}$; see (3.4). A key difference is that for a constant feed rate, the spikes are uniformly distributed in the domain and, as such, there is no preferred location for spike death. This is apparent in Figure 4, where half of the spikes die off when the constant feed rate is decreased below the critical threshold. Contrast this to the nonconstant feed rate (for example, Figure 2(d,e)); spot death there occurs near the minimizer of $A(x)$. More generally, the exact location of spot death depends globally on $A(x)$ in a rather complex way

(see (3.5)). However, for sufficiently variable $A(x)$, spot death is likely to happen near the minimizer of $A(x)$.

In terms of spot birth, one of the key ingredients is the core problem (A.18), which was previously derived for a homogeneous feed rate in a series of papers [33, 26, 29, 30, 20, 21], initially for the related Grey–Scott model [33], of which the Schnakenberg model is a limiting case. Here, we show that the exact same core problem appears for an inhomogeneous feed rate. However, the *outer problem* depends strongly on the inhomogeneity—the second key ingredient. In particular, for a constant feed rate, there is no preferred location for spot creation as the feed rate is increased (see, for example, Figure 1(b) in [20]). Contrast this to the nonconstant feed rate (for example, Figure 2(b,c)). Our results show that as $A(x)$ is gradually increased, spot creation first occurs at a location where the feed rate $A(x)$ is at a maximum.

Using mean-limit approximations, we found the upper and lower bounds for the number of stable spikes—see (3.11). The two bounds coincide when a_0 exceeds $a_{0,\max} \equiv \beta^3/\alpha^2\varepsilon^{-3/2}$. For values of a_0 slightly above $a_{0,\max}$, complex creation-destruction loops can occur, provided that the feed rate $A(x)$ is "sufficiently inhomogeneous" (see Figure 2(f)). However, when $A(x)$ is constant, no such loops occur when $a_0 > a_{0,\max}$. Instead, the solution simply converges to a homogeneous state. Presumably, the destruction and creation of spikes must occur in a different region in order to produce complex creation-destruction loops, which is not the case for a constant feed rate. Further investigation is needed to determine how "inhomogeneous" the feed rate $A(x)$ should be for such loops to exist. In any case, this provides for a nice demonstration that introducing space dependence can lead to completely novel and complex dynamical phenomena that do not occur in the homogeneous case [32].

Until now, there have been very few analytical results about the large-N limit in the literature. In two dimensions, a prominent example is the Gross–Pitaevskii equation used to model Bose–Einstein condensates, whose solutions consist of vortex-like structures [47, 1, 4]. For a two-dimensional trap, an asymptotic reduction for motion of vortex centers yields an interacting particle system [46, 3, 49], which in turn can be reformulated as a nonlocal PDE in the continuum limit of many vortices [37, 18]. While the analysis is quite different from the present paper, the end result is similar: one obtains instability thresholds which yield the maximum number of allowable vortices as a function of trap rotation rate and its chemical potential.

We used formal asymptotics, in the double limit of $\varepsilon \to 0$ and $N \to \infty$, to derive the results in this paper. There are numerous issues of convergence and rigor which this paper does not address, except to verify the results using numerics to compare with the original PDE system. It would be an interesting (and sometimes formidable) challenge to obtain error estimates and rigorously prove convergence of our results.

Numerous other PDE models have solutions that consist of N localized structures that interact in a nonlocal way, and we expect our techniques (with some modifications) to be applicable more widely to other reaction-diffusion systems, such as Gray–Scott and Gierer–Meinhardt [32, 45], and more generally to other physical systems. The key takeaway message is that when the number of localized structures becomes large, a mean-field approach can yield important insights that cannot easily be obtained from looking at the finite-N situation. We hope that readers can attempt such an approach on their own systems.

Appendix A. ODEs for Spike Centers and the Core Problem. Here we derive the reduced system for the motion of spike centers of the system (2.2), i.e., Proposition 2.1. The procedure is relatively standard. It consists of computing outer and inner

solutions, using a solvability condition, and matching. In the derivation below, we assume for simplicity that $A(x)$ is even although it generalizes easily to arbitrary $A(x)$.

Inner Solution. Near the kth spike we expand

$$u(x) = U(y), \quad v(x) = V(y), \quad y = \frac{x - x_k(t)}{\varepsilon}, \quad s = t,$$

so that

$$-\varepsilon U_y x_k' = U_{yy} - U + U^2 V, \qquad 0 = V_{yy} + \varepsilon^2 a_0 A(x) - \varepsilon U^2 V.$$

Next we expand

$$U = U_0 + \varepsilon U_1 + \cdots, \quad V = V_0 + \varepsilon V_1 + \cdots.$$

At the leading order we obtain

$$0 = U_{0yy} - U_0 + U_0^2 V_0, \qquad 0 = V_{0yy}. \tag{A.1}$$

The solution for $V_0(y)$ is given by

$$V_0(y) = V_0 + \alpha y. \tag{A.2}$$

However, as we will show below (see discussion following (A.13)), matching the inner and outer solutions will yield $\alpha = 0$. It then follows that

$$V_0(y) = V_0, \quad U_0(y) = w(y)/V_0, \tag{A.3}$$

where $V_0 \sim v(x_k)$ will be obtained through inner-outer matching and $w(y)$ is the ground state satisfying

$$w_{yy} - w + w^2 = 0, \quad w'(0) = 0, \quad w(y) \to 0 \text{ as } y \to \pm\infty. \tag{A.4}$$

It is well known that the solution to (A.4) is given by

$$w(y) = \frac{3}{2}\operatorname{sech}^2(y/2). \tag{A.5}$$

The next-order equations are

$$-x'(t)U_{0y} = U_{1yy} - U_1 + 2wU_1 + U_0^2 V_1, \tag{A.6}$$

$$V_{1yy} = U_0^2 V_0. \tag{A.7}$$

Multiply (A.6) by U_{0y} and integrate to obtain

$$-x'(t)\int U_{0y}^2 = \int U_0^2 U_{0y} V_1 = -\int \frac{U_0^3}{3} V_{1y}. \tag{A.8}$$

Now

$$V_{1y} = \int_0^y U_0^2 V_0 dy + C,$$

so that (A.8) becomes

$$x'(t) = C\frac{\int U_0^3}{3\int U_{0y}^2} = CV_0\frac{\int w^3}{3\int w_y^2}. \tag{A.9}$$

The constant C is determined as follows:

$$V_{1y}(+\infty) = \int_0^\infty U_0^2 V_0 dy + C, \quad V_{1y}(-\infty) = -\int_0^\infty U_0^2 V_0 dy + C,$$

$$C = \frac{V_{1y}(+\infty) + V_{1y}(-\infty)}{2}. \tag{A.10}$$

Outer Expansion. Away from spike centers, $u(x)$ is assumed to be exponentially small so that $v_{xx} + a_0 A(x) = 0$ for $x \neq x_k$. Near x_k, the term $\frac{u^2 v}{\varepsilon}$ in (1.1) acts like a delta function so that we write

$$v_{xx} + a_0 A(x) \sim \sum_{j=1}^{N} s_j \delta\left(x - x_j\right). \tag{A.11}$$

Here, the weights s_j are defined by

$$s_k \equiv \int_{x_k^-}^{x_k^+} \frac{u^2 v}{\varepsilon} \sim \int_{-\infty}^{\infty} U_0^2 V_0 dy \sim \frac{1}{v_k} \int_{-\infty}^{\infty} w^2(y) dy \sim \frac{6}{v_k},$$

where we defined

$$v_k \equiv v\left(x_k\right).$$

The solution to (A.11) is then given by

$$v(x) = \sum_{j=1}^{N} s_j \frac{|x - x_j|}{2} - a_0 P(x) + mx + c, \tag{A.12}$$

where m, c are constants to be determined and $P(x)$ is defined via

$$P''(x) = A(x), \quad P'(0) = 0. \tag{A.13}$$

At this stage, let us briefly come back to (A.2) to show that, formally, $\alpha = 0$. To do so, we rewrite the outer solution (A.12) in terms of inner variables $x = x_k + \varepsilon y$. Suppose that y is in the intermediate regime, $1 \ll y \ll \varepsilon^{-1}$, so that $x > x_k$. Taylor-expanding (A.12), we then obtain $v(x) = A + B\varepsilon y + O(\varepsilon^2)$, where $A = \sum_{j \neq k} s_j \frac{|x - x_j|}{2} - a_0 P(x_k) + m x_k + c$ and $B = s_k/2 + a_0 P'(x_k) + m$. On the other hand, in the inner region we recall the expansion $V(y) = V_0(y) + \varepsilon V_1(y)$. Matching the two expressions within the intermediate regime $1 \ll y \ll \varepsilon^{-1}$, we obtain $V_0(y) \sim A$, $V_1\left(y\right) \sim By$ in the intermediate regime $1 \ll y \ll \varepsilon$. But we found from (A.1) that $V_0(y) = V_0 + \alpha y$ in the inner region $y \ll \varepsilon^{-1}$. This implies that $V_0 = A$, $\alpha = 0$.

For simplicity, we assume that $A(x)$ is even. In this case the constant m is zero, as can be seen in the following. Compute $v'(\pm L)$ and set it to zero:

$$0 = v'(L) = \sum \frac{s_j}{2} - a_0 P'(L) + m,$$
$$0 = v'(-L) = -\sum \frac{s_j}{2} - a_0 P'(-L) + m.$$

Since P is even, $-P'(-L) = P'(L)$, so that $m = 0$. The expression for c is obtained by integrating (A.11), which yields

$$\int_{-L}^{L} a(x) = \sum s_j.$$

Finally, we also have $v(x_k) = v_k = 6/s_k$. We therefore obtain the following algebraic system for s_k, $k = 1, \ldots, N$ and b:

$$\frac{6}{s_k} = \sum s_j \frac{|x - x_j|}{2} - a_0 P(x) + c, \quad k = 1, \ldots, N, \tag{A.14a}$$

$$\sum s_j = a_0 \int_{-L}^{L} A(x) = 2 a_0 P'(L). \tag{A.14b}$$

To compute $V_{1y}(\pm\infty)$, we match the inner and outer regions. We have

$$V(y) \sim V_0 + \varepsilon V_1(y) \sim v(x_k + \varepsilon y) \sim v(x_k) + \varepsilon y v'(x_k^{\pm}),$$

so that

$$V_{1y}(\pm\infty) = v_x(x_k^{\pm}).$$

We further compute

$$v(x_k^+) = \frac{s_k}{2} + \sum_{j\neq k} \frac{s_j}{2} \frac{x_k - x_j}{|x - x_j|} - a_0 P'(x_k),$$
$$v(x_k^+) = -\frac{s_k}{2} + \sum_{j\neq k} \frac{s_j}{2} \frac{x_k - x_j}{|x - x_j|} - a_0 P'(x_k),$$

so that the constant C in (A.10) evaluates to

$$C = \sum_{j\neq k} \frac{s_j}{2} \frac{x_k - x_j}{|x - x_j|} - a_0 P'(x_k). \tag{A.15}$$

Finally, we have

$$\int_{-\infty}^{\infty} w^2 dy = 6, \quad \int_{-\infty}^{\infty} w^3 dy = \frac{36}{5}, \quad \int_{-\infty}^{\infty} w_y^2 dy = \frac{6}{5},$$

so that (A.9) becomes

$$x_k'(t) = \frac{18}{s_k} \left(\sum_{j\neq k} \frac{s_j}{2} \frac{x_k - x_j}{|x - x_j|} - a_0 P'(x_k) \right), \tag{A.16}$$

subject to $N + 1$ algebraic constraints (A.14). Near x_k, the quasi-steady state is approximated by

$$u \sim w(y)/v_k, \quad v(x_k) \sim v_k, \quad v_k = \frac{6}{s_k}, \quad y = (x - x_k)/\varepsilon.$$

Equations (A.14a), (A.14b), and (A.16) are precisely the equations (2.2) in Proposition 2.1 after rescaling the spike weights and a_0 using the critical scaling

$$a_0 = (b/6)^{-1/2} N^{3/2}, \qquad s_j = (b/6)^{-1/2} N^{1/2} S_j. \tag{A.17}$$

Self-Replication. Next we derive the self-replication thresholds. When s_k is too large, the inner problem becomes fully coupled. The relevant scaling for the inner problem in this case is

$$u = \varepsilon^{-1/2} U, \; v = \varepsilon^{1/2} V, \quad x = x_j + \varepsilon y.$$

The leading-order inner problem for the steady state becomes

$$U_{yy} - U + U^2 V = 0, \quad V_{yy} - U^2 V = 0. \tag{A.18a}$$

We seek an even solution to (A.18a) subject to boundary conditions

$$U(y) \to 0 \text{ as } y \to \infty, \quad V_y(\infty) = B \text{ as } y \to \infty, \quad U'(0) = V'(0) = 0, \tag{A.18b}$$

where the constant B is related to the spike weight s_j as follows. Integrate the second equation in (A.18a) to obtain

$$2B = \int U^2 V dy = \varepsilon^{1/2} s_j. \tag{A.19}$$

The system (A.18) is referred to as the "core problem" and is used to explain the self-replication phenomenon shown in Figure 2(b). It was first identified in [33] in the context of the Gray–Scott model and was further studied in [26, 29, 30, 20, 21].

Numerical computations of the core problem (see, for example, [33, 26]) show that the solution to (A.18) exists only for

$$0 < B < B_c \approx 1.35.$$

As B is increased past B_c, the solution to the core problem disappears as a result of a fold point bifurcation. This disappearance is responsible for the self-replication [26, 29, 30, 20]. Substituting $B = B_c$ into (A.19), we see that the solution exists only if $s_j < 2.70\varepsilon^{-1/2}$. In terms of the rescaled weights S_j (A.17), this yields

$$S_j \le 2.70\varepsilon^{-1/2}\frac{N}{a_0}. \tag{A.20}$$

Acknowledgments. We are grateful to Michael Ward for useful discussions that motivated this problem. We thank the anonymous referees for useful comments that helped to improve the paper.

REFERENCES

[1] J. Abo-Shaeer, C. Raman, J. Vogels, and W. Ketterle, *Observation of vortex lattices in Bose-Einstein condensates*, Science, 292 (2001), pp. 476–479. (Cited on pp. 1, 14)

[2] A. Aftalion, X. Blanc, and J. Dalibard, *Vortex patterns in a fast rotating Bose-Einstein condensate*, Phys. Rev. A, 71 (2005), art. 023611. (Cited on p. 2)

[3] A. Aftalion and Q. Du, *Vortices in a rotating Bose-Einstein condensate: Critical angular velocities and energy diagrams in the Thomas-Fermi regime*, Phys. Rev. A, 64 (2001), art. 063603. (Cited on p. 14)

[4] M. H. Anderson, J. R. Ensher, M. R. Matthews, C. E. Wieman, and E. A. Cornell, *Observation of Bose-Einstein condensation in a dilute atomic vapor*, Science, 269 (1995), pp. 198–201. (Cited on pp. 1, 14)

[5] R. Barrio, C. Varea, J. Aragón, and P. Maini, *A two-dimensional numerical study of spatial pattern formation in interacting Turing systems*, Bull. Math. Biol., 61 (1999), pp. 483–505. (Cited on p. 1)

[6] D. L. Benson, P. K. Maini, and J. A. Sherratt, *Unravelling the Turing bifurcation using spatially varying diffusion coefficients*, J. Math. Biol., 37 (1998), pp. 381–417. (Cited on pp. 2, 12)

[7] D. L. Benson, J. A. Sherratt, and P. K. Maini, *Diffusion driven instability in an inhomogeneous domain*, Bull. Math. Biol., 55 (1993), pp. 365–384. (Cited on p. 12)

[8] S. Chaturapruek, J. Breslau, D. Yazdi, T. Kolokolnikov, and S. G. McCalla, *Crime modeling with Lévy flights*, SIAM J. Appl. Math., 73 (2013), pp. 1703–1720, https://doi.org/10.1137/120895408. (Cited on p. 1)

[9] Y. Chen, T. Kolokolnikov, J. Tzou, and C. Gai, *Patterned vegetation, tipping points, and the rate of climate change*, European J. Appl. Math., 26 (2015), pp. 945–958. (Cited on pp. 1, 2)

[10] M. C. Cross and P. C. Hohenberg, *Pattern formation outside of equilibrium*, Rev. Modern Phys., 65 (1993), pp. 851–1112. (Cited on p. 2)

[11] F. Dalfovo, S. Giorgini, L. P. Pitaevskii, and S. Stringari, *Theory of Bose-Einstein condensation in trapped gases*, Rev. Modern Phys., 71 (1999), pp. 463–512. (Cited on p. 2)

[12] P. De Kepper, I. R. Epstein, K. Kustin, and M. Orban, *Systematic design of chemical oscillators. Part 8. Batch oscillations and spatial wave patterns in chlorite oscillating systems*, J. Phys. Chem., 86 (1982), pp. 170–171. (Cited on p. 1)

[13] D. Iron and M. J. Ward, *The dynamics of multispike solutions to the one-dimensional Gierer–Meinhardt model*, SIAM J. Appl. Math., 62 (2002), pp. 1924–1951, https://doi.org/10.1137/S0036139901393676. (Cited on pp. 4, 13)

[14] D. Iron, M. J. Ward, and J. Wei, *The stability of spike solutions to the one-dimensional Gierer–Meinhardt model*, Phys. D, 150 (2001), pp. 25–62. (Cited on p. 13)

[15] D. Iron, J. Wei, and M. Winter, *Stability analysis of Turing patterns generated by the Schnakenberg model*, J. Math. Biol., 49 (2004), pp. 358–390. (Cited on pp. 2, 3, 10, 13)

[16] P. G. Kevrekidis, D. J. Frantzeskakis, and R. Carretero-González, *Emergent Nonlinear Phenomena in Bose-Einstein Condensates: Theory and Experiment*, Vol. 45, Springer Science & Business Media, 2007. (Cited on p. 2)

[17] C. A. Klausmeier, *Regular and irregular patterns in semiarid vegetation*, Science, 284 (1999), pp. 1826–1828. (Cited on p. 1)

[18] T. Kolokolnikov, P. Kevrekidis, and R. Carretero-González, *A tale of two distributions: From few to many vortices in quasi-two-dimensional Bose–Einstein condensates*, Proc. R. Soc. Lond. Ser. A Math. Phys. Eng. Sci., 470 (2014), art. 20140048. (Cited on pp. 2, 14)

[19] T. Kolokolnikov and M. Tlidi, *Spot deformation and replication in the two-dimensional Belousov-Zhabotinski reaction in a water-in-oil microemulsion*, Phys. Rev. Lett., 98 (2007), art. 188303. (Cited on p. 1)

[20] T. Kolokolnikov, M. J. Ward, and J. Wei, *The existence and stability of spike equilibria in the one-dimensional Gray–Scott model: The pulse-splitting regime*, Phys. D, 202 (2005), pp. 258–293. (Cited on pp. 9, 14, 18)

[21] T. Kolokolnikov, M. J. Ward, and J. Wei, *Spot self-replication and dynamics for the Schnakenburg model in a two-dimensional domain*, J. Nonlinear Sci., 19 (2009), pp. 1–56. (Cited on pp. 9, 14, 18)

[22] T. Kolokolnikov, M. J. Ward, and J. Wei, *The stability of steady-state hot-spot patterns for a reaction-diffusion model of urban crime*, Discrete Contin. Dyn. Syst. Ser. B, 19 (2014), pp. 1373–1410. (Cited on p. 1)

[23] S. Kondo and R. Asai, *A reaction-diffusion wave on the skin of the marine angelfish* Pomacanthus, Nature, 376 (1995), pp. 765–768. (Cited on p. 1)

[24] A. Madzvamuse, A. J. Wathen, and P. K. Maini, *A moving grid finite element method applied to a model biological pattern generator*, J. Comput. Phys., 190 (2003), pp. 478–500. (Cited on p. 2)

[25] P. K. Maini, T. E. Woolley, R. E. Baker, E. A. Gaffney, and S. S. Lee, *Turing's model for biological pattern formation and the robustness problem*, Interface Focus, 2 (2012), pp. 487–496, art. rsfs20110113. (Cited on p. 1)

[26] C. Muratov and V. Osipov, *Spike autosolitons and pattern formation scenarios in the two-dimensional Gray-Scott model*, Eur. Phys. J. B, 22 (2001), pp. 213–221. (Cited on pp. 9, 14, 18)

[27] J. Murray, *Why are there no* 3*-headed monsters? Mathematical modeling in biology*, Notices Amer. Math. Soc., 59 (2012), pp. 785–795. (Cited on p. 2)

[28] J. D. Murray, *Mathematical Biology.* II *Spatial Models and Biomedical Applications*, Interdiscip. Appl. Math. 18, Springer-Verlag, New York. 2001. (Cited on p. 2)

[29] Y. Nishiura and D. Ueyama, *A skeleton structure of self-replicating dynamics*, Phys. D, 130 (1999), pp. 73–104. (Cited on pp. 9, 14, 18)

[30] Y. Nishiura and D. Ueyama, *Spatio-temporal chaos for the Gray–Scott model*, Phys. D, 150 (2001), pp. 137–162. (Cited on pp. 9, 14, 18)

[31] Q. Ouyang and H. L. Swinney, *Transition from a uniform state to hexagonal and striped Turing patterns*, Nature, 352 (1991), pp. 610–612. (Cited on p. 1)

[32] K. M. Page, P. K. Maini, and N. A. Monk, *Complex pattern formation in reaction–diffusion systems with spatially varying parameters*, Phys. D, 202 (2005), pp. 95–115. (Cited on pp. 2, 3, 14)

[33] J. E. Pearson, *Complex patterns in a simple system*, Science, 261 (1993), pp. 189–192. (Cited on pp. 9, 14, 18)

[34] L. P. Pitaevskii and S. Stringari, *Bose-Einstein Condensation*, Internat. Ser. Monogr. Phys. 116, Oxford University Press, 2003. (Cited on p. 2)

[35] R. G. Plaza, F. Sanchez-Garduno, P. Padilla, R. A. Barrio, and P. K. Maini, *The effect of growth and curvature on pattern formation*, J. Dynam. Differential Equations, 16 (2004), pp. 1093–1121. (Cited on p. 2)

[36] J. Schnakenberg, *Simple chemical reaction systems with limit cycle behaviour*, J. Theoret. Biol., 81 (1979), pp. 389–400. (Cited on p. 2)

[37] D. E. Sheehy and L. Radzihovsky, *Vortex lattice inhomogeneity in spatially inhomogeneous superfluids*, Phys. Rev. A, 70 (2004), art. 051602. (Cited on pp. 2, 14)

[38] J. A. Sherratt, *An analysis of vegetation stripe formation in semi-arid landscapes*, J. Math. Biol., 51 (2005), pp. 183–197. (Cited on p. 1)
[39] J. A. Sherratt, *Using wavelength and slope to infer the historical origin of semiarid vegetation bands*, Proc. Natl. Acad. Sci., 112 (2015), pp. 4202–4207. (Cited on p. 2)
[40] J. A. Sherratt and G. J. Lord, *Nonlinear dynamics and pattern bifurcations in a model for vegetation stripes in semi-arid environments*, Theoret. Population Biol., 71 (2007), pp. 1–11. (Cited on p. 1)
[41] M. B. Short, M. R. D'orsogna, V. B. Pasour, G. E. Tita, P. J. Brantingham, A. L. Bertozzi, and L. B. Chayes, *A statistical model of criminal behavior*, Math. Models Methods Appl. Sci., 18 (2008), pp. 1249–1267. (Cited on p. 1)
[42] K. Siteur, E. Siero, M. B. Eppinga, J. D. Rademacher, A. Doelman, and M. Rietkerk, *Beyond Turing: The response of patterned ecosystems to environmental change*, Ecological Complexity, 20 (2014), pp. 81–96. (Cited on p. 2)
[43] M. J. Ward and J. Wei, *The existence and stability of asymmetric spike patterns for the Schnakenberg model*, Stud. Appl. Math., 109 (2002), pp. 229–264. (Cited on pp. 2, 3, 10, 13)
[44] J. Wei and M. Winter, *Mathematical Aspects of Pattern Formation in Biological Systems*, Appl. Math. Sci. 189, Springer Science & Business Media, 2013. (Cited on p. 2)
[45] J. Wei and M. Winter, *Stable spike clusters for the one-dimensional Gierer-Meinhardt system*, European J. Appl. Math., 28 (2017), pp. 576–635. (Cited on pp. 2, 14)
[46] E. Weinan, *Dynamics of vortex liquids in Ginzburg-Landau theories with applications to superconductivity*, Phys. Rev. B, 50 (1994), pp. 1126–1135. (Cited on p. 14)
[47] S. Xie, P. Kevrekidis, and T. Kolokolnikov, *Multi-vortex crystal lattices in Bose-Einstein condensates with a rotating trap*, submitted. (Cited on p. 14)
[48] S. Xie and T. Kolokolnikov, *Moving and jumping spot in a two dimensional reaction diffusion model*, Nonlinearity, 30 (2017), pp. 1536–1563. (Cited on p. 3)
[49] D. Yan, R. Carretero-González, D. Frantzeskakis, P. Kevrekidis, N. Proukakis, and D. Spirn, *Exploring vortex dynamics in the presence of dissipation: Analytical and numerical results*, Phys. Rev. A, 89 (2014), art. 043613. (Cited on p. 14)
[50] J. R. Zipkin, M. B. Short, and A. L. Bertozzi, *Cops on the dots in a mathematical model of urban crime and police response*, Discrete Contin. Dyn. Syst. Ser. B, 19 (2014), pp. 1479–1506. (Cited on p. 1)

AQ